Featuring work from the Microsystems Laboratory of Dr Ana Valero in the Institute of Microengineering and Center of MicroNanoTechnology at the Ecole Polytechnique Federal de Lausanne, Switzerland.

Title: A unified approach to dielectric single cell analysis: Impedance and dielectrophoretic force spectroscopy

Single cell dielectric spectroscopy is a powerful tool for label-free analysis and characterization of biological cells. This paper presents a microfabricated flow-cytometer and a cell-sorting microdevice capable of measuring the spectral impedance of individual cells as well as discriminating between cell types according to their dielectric properties, aimed at diagnostic applications for cell counting and separation in hematology, oncology or toxicology.

As featured in:

See Valero *et al.*, *Lab Chip,* 2010, **10**, 2216–2225

RSCPublishing

www.rsc.org
Registered Charity Number 207890

A unified approach to dielectric single cell analysis: Impedance and dielectrophoretic force spectroscopy†‡

Ana Valero,* Thomas Braschler and Philippe Renaud

In this review we present a unified approach for single cell dielectric spectroscopy. Impedance spectroscopy and dielectrophoretic cell sorting, current microtechnologies applied in electrical analysis of single cells are discussed based on their closely related physical principles. In addition, examples of microfluidic devices will be presented: a microfabricated flow cytometer for single cell discrimination based on impedance analysis and a miniaturized continuous dielectrophoretic cell sorter, both using the concept of liquid electrodes. Using the experimental results obtained from both microdevices, we give a comparative overview over the dielectrophoretic sorting and impedance spectroscopy.

1. Introduction

In the past two decades the development of new micro-technologies for biological and chemical analysis has become a major area of interest. Label-free and non-invasive techniques are particularly promising in the analysis of primary materials of limited availability and complex composition.

Electrical analysis of biological cells has drawn special attention in this field. The know-how on recording and processing of electronic signals, the readily available technology for miniaturization and on chip integration, and the possibility to avoid cell labelling make it a very attractive, powerful and competitive

method in areas such as disease diagnosis,[1–3] food safety,[4] environmental monitoring,[5] drug screening[6–8] as well as in cellular biology[9] and neuroscience.[10–12]

Impedance spectroscopy is a powerful tool for label-free analysis and characterization of biological cells,[13–18] providing information on membrane capacitance and resistance and cytoplasm conductivity and permittivity.[19–22] The first cytometer capable of measuring the electrical properties of single cells was developed by Coulter.[13] It measures a change in DC resistance when a cell passes through a small orifice connecting two otherwise electrically isolated fluid filled chambers. Currently, numerous novel approaches for dielectric measurement of individual single cells at high speed have been developed as a result of the technological advances in microfluidics, microelectronics and electrophysiology. Flow impedance measurement of cells in miniaturized devices offers many advantages over conventional techniques, such as high sensitivity, sample size reduction, integration of reference measurement electrodes, the use of sheath flow or dielectrophoretic forces for cell centring and the possibility of *in situ* implementation of cell sorting.[23] The first

Microsystems Laboratory, Ecole Polytechnique Federale de Lausanne, EPFL, BM 3.124 Station 17, Lausanne, Switzerland. E-mail: ana. valero@epfl.ch

† Electronic supplementary information (ESI) available: Impedance model for the Maxwell–Garnett mixing equation. See DOI: 10.1039/c003982a

‡ Published as part of a themed issue dedicated to Swiss Research: Guest Editor Professor Viola Vogel.

Ana Valero

Ana Valero received her MSc in Chemistry in 2001 at the University of Zaragoza. In 2002 she started her PhD in electrical engineering at the BIOS/Lab on a chip group of the MESA+ Institute at Twente University, under the supervision of Prof. Albert van den Berg. In 2007 she moved to Switzerland where she started her PostDoc with Prof. Philippe Renaud at EPFL, Ecole Polytechnique Federal Lausanne, where she is currently working. Her research interests include single cells on chips, separation devices, microanalysis systems and diagnosis on chip.
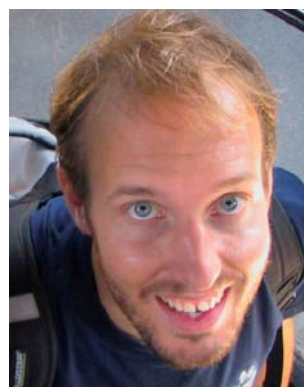
Thomas Braschler

Thomas Braschler received his MSc in Biology in 2002 at the University of Lausanne. In 2003 he started his PhD in the Laboratory of Microsystems, at the Ecole Polytechnique Federal de Lausanne (EPFL) under the supervision of Prof. Philipp Renaud, concerning microfluidic devices for cell entrapment in hydrogels and for cell sorting by dielectrophoresis. Currently, he is a postdoc at the Hospital of Lausanne (CHUV) at the department of ophthalmology, doing research on stem cells of the eye cornea. His research interest include single cells on chips, hydrogels, micro- and nano separation devices.

microfluidic device with integrated electrodes showed the potential for discriminating single erythrocytes from leuko-cytes.[24] Since then different designs of micro-cytometers have been fabricated capable of measuring the optical and/or electrical properties of single particles.[14,23–35]

Cell sorting based on dielectrophoresis (DEP),[36,37] also makes use of the distinctive dielectric properties of cells. DEP is the force arising on a dielectric particle subjected to a non-uniform electric field. DEP-based methods are suitable and potentially powerful for the integration on chip of continuous-flow separa-tion since they directly yield sorted populations. We have recently developed an equilibrium-based continuous cell sorter based on dielectrophoresis.[38–40] In this case, the dielectric prop-erties of the cells can be reconstructed from the position of the particle stream after the active element. DEP-based manipula-tions are non-invasive and prevent cell damage when limited to reasonable electric field strengths.[41] In general, integrated sample separation and analysis are potentially less time consuming, less invasive and more sensitive than conventional tests. In addition to our equilibrium-based sorting device, numerous examples of cell sorter microdevices based on dielectrophoresis have been reported in the literature; major techniques are stop-flow frac-tionation,[42–45] field-flow fractionation (FFF),[46–50] electrodeless dielectrophoresis[51–55] or traveling wave dielectrophoresis.[56–58]

The scope of this paper is to give a comprehensive and detailed overview of the developments achieved in dielectric flow cytom-etry at our laboratory, and in particular the comparison of impedance spectroscopy and dielectrophoretic sorting. We first discuss the theory and background of the two techniques, focusing on the common physical basis. Next, we present two different microdevices developed at our laboratory, a microfabricated flow cytometer for single cell discrimination based on impedance analysis and a miniaturized continuous dielectrophoretic cell sorter. Using the experimental results obtained within both microdevices for the detection and separation of *Babesia bovis* infected red blood cells as an experimental example, we give a comparative overview over the two techniques. Further appli-cations of impedance spectroscopy developed at our laboratory include characterisation of red blood cells and ghosts cells, monitoring of cell changes upon fixation as well as cell counting after dielectrophoretic separation. Applications of the equilib-rium dielectrophoretic sorter include separation of viable from non-viable cells as well as synchronization of a yeast cell culture.

2. Theory

Biological cells, in impedance measurements or dielectric sorting, can be modeled as dielectric particles that get polarized in the presence of an electric field. Interfacial polarization occurs when a heterogeneous dielectric system, *e.g.* a biological cell in a physiological solution, is subjected to an electric field.[59–62] The polarization, defined as the dipole moment per unit volume, p, is related to the effective permittivity of the system $\tilde{\varepsilon}$ and the electric field E, according to:

$$p = \tilde{\varepsilon} \cdot E \qquad (1)$$

For a homogeneous medium in an AC electric field with angular frequency ω, the effective permittivity will have both a real part and imaginary part, reflecting charge storage in and out of phase with the electric field respectively:

$$\tilde{\varepsilon}_m = \varepsilon_m - \sigma_m \big/ j\omega \qquad (2)$$

In the upper kHz and lower MHz range and near-physiolog-ical solutions typically used in impedance spectroscopy, the real part is mainly due to the movement of bound charges, whereas the imaginary part arises from the electrical current carried by the mobile charges.

In the presence of suspended particles, in our case biological cells, the effective permittivity is given by the Maxwell–Garnett mixing equation:

$$\tilde{\varepsilon} = \tilde{\varepsilon}_m \cdot \frac{1 + 2 \cdot \phi \cdot f_{CM}(\omega)}{1 - \phi \cdot f_{CM}(\omega)} \approx \tilde{\varepsilon}_m \cdot (1 + 3 \cdot \phi \cdot f_{CM}(\omega)) \qquad (3)$$

where ϕ is the volume fraction occupied by the cells, and $f_{CM}(\omega)$ is the Clausius–Mossotti factor, characterizing the cells' dielec-tric response. The approximation in eqn (3) indicates that at low volume fractions, the cells contribute an essentially additive dipole moment, given by:

$$\Delta p = E \cdot \Delta \tilde{\varepsilon} = 3 \cdot \phi \cdot f_{CM} \cdot \tilde{\varepsilon}_m E \qquad (4)$$

In impedance spectroscopy, we quantify the change in $\tilde{\varepsilon}$ arising from this additional dipole moment. The impedance is related inversely to the complex permittivity of a sample:

$$Z = \frac{\kappa}{j\omega\tilde{\varepsilon}} \approx \frac{\kappa}{j\omega\tilde{\varepsilon}_m} \cdot (1 - 3 \cdot \phi \cdot f_{CM}) \qquad (5)$$

κ being the geometric cell constant of the measurement volume. Since the impedance of the medium alone is given by $Z_0 = \frac{\kappa}{j\omega\tilde{\varepsilon}_m}$, we have for the relative impedance change due to the presence of a cell:

Philippe Renaud

Philippe Renaud received his PhD degree in Physics from the University of Lausanne, Swit-zerland in 1988. He was post-doctoral researcher at University of California in Ber-keley, USA to develop scanning tunneling microscopes for low temperature and at the IBM Zürich Research laboratory where he performed measure-ments of the local STM induced luminescence. He then joined the Sensors and Actuators group of the Swiss Center for Electronics and Microtechnology (CSEM) at Neuchâtel where he was involved in the design and the tech-nology of microsensors and micro-mirrors for optical switching. In 1993, he joined EPFL as assistant professor but remained a part-time collaborator of CSEM until the end of 1994. In the summer of 1996, he went to Japan as visiting professor at the Tohoku University. In 1997, he was appointed as full professor at EPFL. His research interests are microfluidics and BioMEMS applica-tions.

$$\frac{\Delta Z}{Z_0} = \frac{Z - Z_0}{Z_0} \approx -3 \cdot \phi \cdot f_{CM} \quad (6)$$

In dielectric sorting, we quantify the force acting on the particles, which for spherical particles is given by:

$$F_{DEP} = \langle (P \cdot \nabla)E \rangle = \frac{3\pi}{2}\varepsilon_m V \cdot \mathrm{Re}(f_{CM})\nabla|E_{rms}|^2 \quad (7)$$

where $V = 4\pi/3r^3$ is the volume of a spherical particle with radius r. Eqn (7) shows that dielectrophoresis depends on the induced dipole moment $P = pV$.

Both impedance measurements and the dielectrophoretic force are governed by the Clausius–Mossotti factor f_{CM}. The Clausius–Mossotti factor quantifies the dipole moment induced in a suspended particle relative to the dipole moment that would be induced in an equivalent volume of suspension medium. It fully characterizes the particle's dielectric response, and can be expressed as follows:

$$f_{CM}(\omega) = \frac{\tilde{\varepsilon}_p - \tilde{\varepsilon}_m}{\tilde{\varepsilon}_p + 2 \cdot \tilde{\varepsilon}_m} \quad (8)$$

It follows from eqn (7) that it is the difference in complex permittivity between the particles or cells ($\tilde{\varepsilon}_p$) and the medium ($\tilde{\varepsilon}_m$) that is responsible for the appearance of an additional net induced dipole in the presence of particles.

The real part of the Clausius–Mossotti factor f_{CM} is bounded by -0.5 and 1 according to whether the medium polarizability or the particle polarizability dominates in eqn (8). So taking the force on highly polarisable particle with dimensions identical to the cell as a reference force F_0, we can normalize the DEP force:

$$\frac{F_{DEP}}{F_0} = \mathrm{Re}(f_{CM}) \quad (9)$$

An important difference between impedance measurements and dielectrophoresis is highlighted by eqn (9) as compared to eqn (6): Classical dielectrophoresis can be used to determine the real part of the Clausius–Mossotti factor only, whereas impedance measurements also yield phase information and therefore both the real and imaginary part of the Clausius–Mossotti factor.

If the particle is a homogeneous sphere, eqn (2) and eqn (8) can directly be employed to calculate f_{CM}. Biological cells however are not homogeneous spheres, the high contrast of conductivity between cytoplasm and the isolating membrane makes it necessary to consider at least a core–shell model. To obtain the effective complex permittivity of such a compound particle, a mixing equation is needed:[63]

$$\tilde{\varepsilon}_{effective} = \tilde{\varepsilon}_{outer} \cdot \frac{\left(\frac{r_{outer}}{r_{inner}}\right)^3 + 2\dfrac{\tilde{\varepsilon}_{inner} - \tilde{\varepsilon}_{inner}}{\tilde{\varepsilon}_{inner} + 2\tilde{\varepsilon}_{inner}}}{\left(\frac{r_{outer}}{r_{inner}}\right)^3 - \dfrac{\tilde{\varepsilon}_{inner} - \tilde{\varepsilon}_{outer}}{\tilde{\varepsilon}_{inner} + 2\tilde{\varepsilon}_{outer}}} \quad (10)$$

where r_{outer} is the radius of the entire particle (shell + core) and r_{inner} designates the radius of the core. $\tilde{\varepsilon}_{outer}$ and $\tilde{\varepsilon}_{inner}$ designate the complex permittivities of the shell and core respectively.

The theoretical relation between the complex permittivity, the real part of the Clausius–Mossotti factor, the physical DEP force and the impedance curve of a cell suspension is shown in comparison in Fig. 1. In the low frequency range, the cell
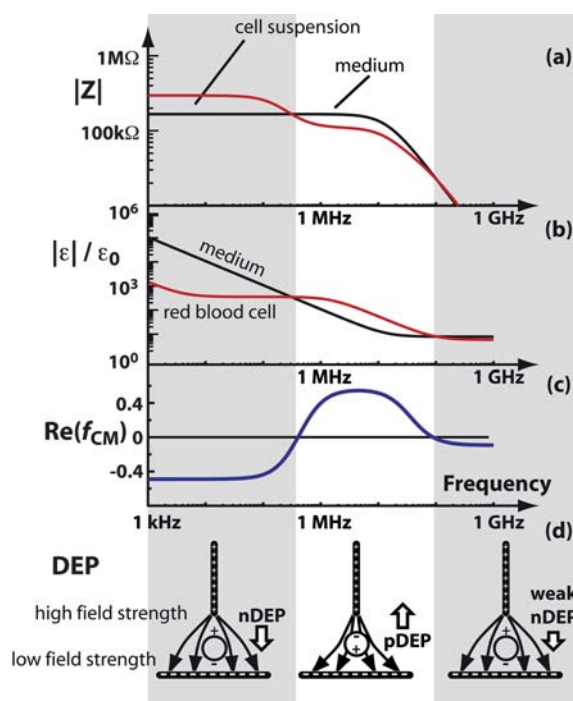
Fig. 1 Impedance, complex permittivity, Clausius-Mossotti factor and dielectrophoretic force in comparison. The complex permittivity of the medium and the red blood cell modeled as a single shell spherical particle are both frequency dependent, but not in an identical way (Fig. 1b); the presence of the cells is also reflected in the impedance (Fig. 1a). The Clausius–Mossotti factor governs impedance, complex permittivity and dielectrophoretic behaviour. Its real value, relevant for the dielectrophoresis, changes from negative to positive and back to negative values for the frequency range considered (c). As a consequence, the dielectrophoretic force in an inhomogeneous field, as shown in part (d), changes from nDEP to pDEP and back to nDEP over the frequency range considered. The model parameters are: $\sigma_m = 60$ mS m^{-1}, $\varepsilon_m = 78$ ε_0; the red blood cell is modeled with a single shell model, that is cytoplasm + membrane. The cytoplasmic conductivity and permittivity are 310 mS m^{-1} and 59 ε_0, whereas the membrane is assumed to be 4.5 nm thick, of a conductivity of 1 μS m^{-1} and a permittivity of 4.44 ε_0. The red blood cell parameters are taken from ref. 74 whereas the medium conductivity corresponds to the low-conductivity buffer typically used in cell sorting experiments (60 mS m^{-1}). For the impedance curve, a volume fraction of 30% for the red blood cells is assumed.

membrane acts as an efficient insulator, and the current is forced to flow around the cell. The complex permittivity for the cell is lower than the one for the medium, the impedance is essentially the same as the one of a completely isolating particle of the same shape, giving rise to a negative Clausius–Mossotti factor and hence to nDEP forces, repulsing the cell from the high field strength region. With increasing frequency, capacitive current flow across the cell membrane becomes more and more efficient compared with ohmic flow around the cell, and the difference between cell and medium permittivity diminishes. When the frequency of the excitation signal is increased above a first crossover frequency (in Fig. 1 about 400 kHz) the current flow through the cell becomes higher than through equivalent regions of surrounding medium, since in this case the medium is chosen to be substantially less conductive than the cell interior. Accordingly, the real part of the Clausius–Mossotti factor

becomes positive and attraction of the cells to high field strength regions by pDEP takes place. Since the electric current in this high frequency region probes the cell interior, we can use a high frequency signal to probe the intracellular space and therefore to discriminate between different cell types or different physiological states of the same cell type or to detect the presence of intracellular parasite.

Towards the GHz frequency range, capacitive current flow by bulk reorientation of the aqueous solution becomes more efficient than conductive current flow. The complex permittivity then reaches the plateau value between β and δ dispersion in terms of the dielectric relaxation theory.[64] Since the macromolecular constituents of the cell interior reorient somewhat less easily with the field cycles than the free water molecules, the permittivity of the cells in this region is somewhat less than the one of the medium. So above a second cross-over frequency of about 90 MHz for the model prediction in Fig. 1, we enter again in a nDEP regime.

Impedance changes due to the presence of a particle and dielectrophoretic phenomena are both due to the induced dipoles. In the case of the impedance measurement, the induced dipole is detected *via* its electric field, superimposing itself on the primary applied voltage or current. In dielectrophoresis, the induced dipole experiences a force in the inhomogeneous field, leading to particle displacement. The analogy between impedance measurements and dielectrophoretic forces also has a useful consequence in practice: the complex permittivities can be obtained from equivalent electrical circuits. Discrete models are more intuitive than the Maxwell–Garnett mixing equation or the multi-shell recursion relation, and are therefore helpful in interpreting the electric behaviour of cells and other particles. Moreover, discrete models involving only a few capacitive and resistive elements can give very good approximations to the Maxwell–Garnett mixing equation.[65]
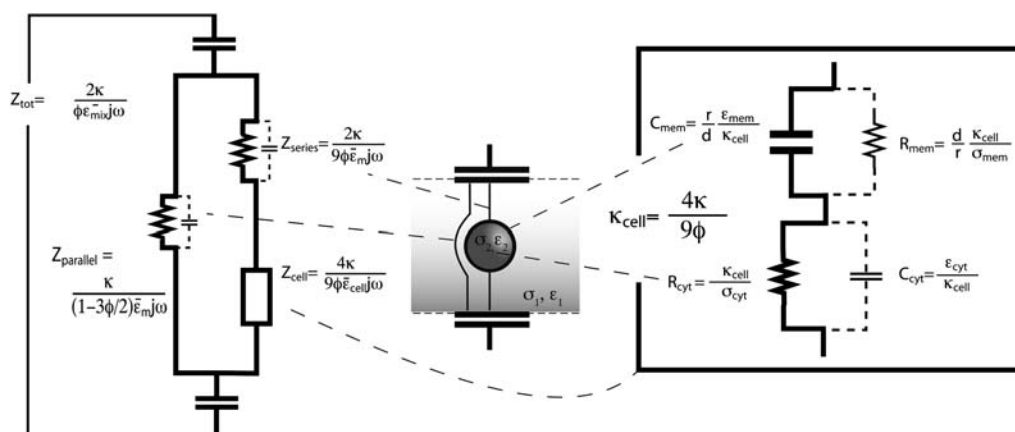
Fig. 2 shows a discrete electric equivalent model of a biological cell in suspension. The principal current paths through and around a cell, as well as the associated impedance formulas are shown. The highlighted current paths are particularly important in the region of the β dispersion:[23] when going from low to high

frequency, we enter the β dispersion when capacitive current flow through the cell membrane becomes important compared to resistive current flow around the cell; at that moment, the current also starts to probe efficiently the cell interior, in particular its conductance.

Whereas considering the cell and its immediate surroundings as shown in Fig. 2 is enough to model the dielectrophoretic response, in impedance spectroscopy we would also have to consider the limited capacity of microelectrodes to couple current into a solution, that is, we have to add the electrical double layer impedance of the microelectrodes. The formulae indicated in Fig. 2 approximate the Maxwell–Garnett mixing equation (eqn (3)) and the single-shell model for the cell (eqn (10)) and they are adapted from ref. 65. The exact development for the single-shell equivalent model and for the general model shown in Fig. 2 can be found in the ESI(S1 and S2†).

3. Impedance spectroscopy in a micro flow cytometer

The impedance spectroscopy approach is particularly suited to operate at the micrometre scale, which permits the analysis of single cell dielectric properties. In our laboratory, a new cytological tool based on the micro Coulter particle counter (µCPC) principle was developed aiming at diagnostic applications for cell counting and separation in hematology, oncology or toxicology. The device measures the spectral impedance of individual cells or particles and allows screening rates over 100 samples s^{-1} on a single-cell basis. The device is based on the concept of liquid electrodes: large metal electrodes are situated in lateral chambers. The electric field is then conducted to the main measurement channel by comparatively narrow access channels. This ensures a homogeneous distribution of the field strength and hence sensitivity across the channel height, while still allowing for a planar fabrication strategy. A laminar liquid flow carries the suspended particles through the measurement area. Each particle's impedance signal is recorded by a differential pair of microelectrodes using the cell surrounding media as a reference (Fig. 3a). The micromachined chip and processing electronic circuit allow simultaneous impedance measurements at multiple

Fig. 2 Discrete electric equivalent circuit model of a biological cell in suspension, taking into account cell membrane, cytoplasmic conductivity σ_2 and permittivity ε_2, medium conductivity σ_1 and permittivity ε_1 and electrical double layer impedance of the miroelectrodes. The main current paths through and around the cell and the associated impedance formulas are shown. The current paths that are particularly important in the β-dispersion region are highlighted.

a) Measurement Principle

b) Sensitivity Analysis
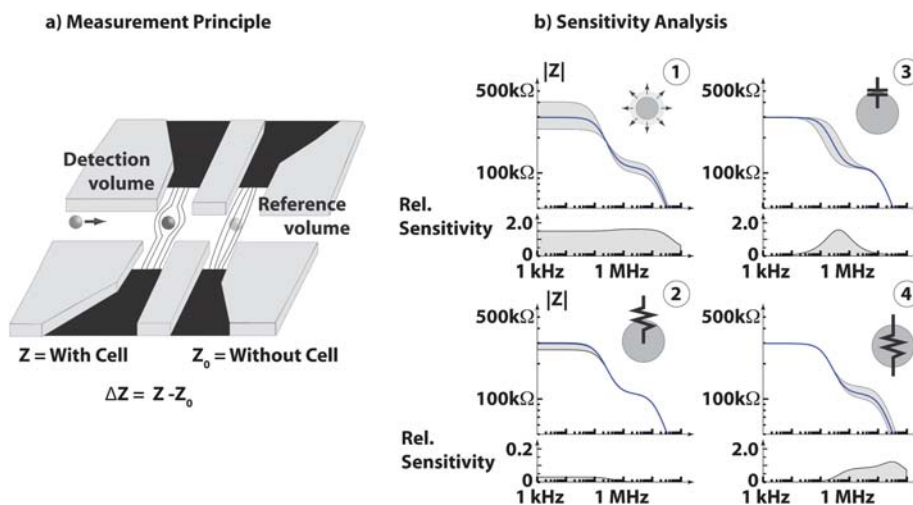
Fig. 3 (a) Schematic of the microfluidic flow cytometer device and cell detection principle; the detection and reference volumes are inherently switched as the cell passes through each. Z_0 is the impedance of the solution-filled channel of complex conductivity σ1 and ε1. Z is the impedance with a cell present. ΔZ is defined as the impedance difference between these two states $\Delta Z = Z - Z_0$. (b) Illustration of the effect of changing different model parameters on the impedance. The calculations are carried out without taking the electrode interfacial impedance into account. The model parameters are identical to the ones used for Fig. 1, except for the variations for the individual panel. In general, in order to illustrate the changes in the absolute value of $|Z|$ due to each parameter, large variations of the corresponding parameter were used, whereas for the sensitivity curve shown in the lower part of the individual panels, small variations were used. In panel 1, the volume fraction ϕ is varied from 20% to 40%; the sensitivity curve is obtained as $|\Delta Z/Z|/\phi$ for $\phi = 1\%$. In panel 2, for the $|Z|$-curve the membrane conductivity was changed by a factor of 10 and 0.1, whereas for the sensitivity curve it was changed by 1%; the sensitivity is defined as $|\Delta Z/Z|/\phi$ divided by the relative change of the membrane resistivity (*i.e.* 0.01). In panel 3, for the $|Z|$-curve the membrane capacitance was changed by a factor of 2 and 0.5, whereas for the sensitivity curve it was changed by 1%; the sensitivity is defined as $|\Delta Z/Z|/\phi$ divided by the relative change of the capacitance (*i.e.* 0.01).). In panel 4, for the $|Z|$-curve the cytosol resistivity was changed by a factor of 2 and 0.5, whereas for the sensitivity curve it was changed by 1%; the sensitivity is defined as $|\Delta Z/Z|/\phi$ divided by the relative change of the cytosol resistance (*i.e.* 0.01).

frequencies, typically ranging from 100 kHz to 15 MHz. Interrogating the cell simultaneously at different frequencies of interest can thus bring a wealth of information which is presently available only with slower or more expensive instruments. Although other electrode configurations, *e.g.* top and bottom, or up- and downstream electrode geometries, give a somewhat higher relative impedance change (as shown by FEM simulations[14]) the design described here was preferred due to simplicity in the microfabrication steps and the robustness of large electrodes located relatively far away from the flowing cells.

The liquid electrode strategy solves several problems commonly encountered when downscaling the microfluidic channels and embedding microelectrodes. First, small electrodes imply small electrode double layer capacitance and hence high electrode interfacial impedance, in particular at low frequency. This typically limits of the useful frequency range to 100 kHz and above, thus placing stringent constraints on the detection technique as well as the signalling amplification. With liquid electrodes, we could detect the passage of cells down to 0.1 kHz without special precaution. Second, microelectrodes on the size scale of single cells are easily damaged by electrochemical reactions or deposition of cell debris, whereas the large metal patches used in the liquid electrodes are essentially immune to these problems. And third, since the field in the measurement region is horizontal and perpendicular to the flow, hydrodynamic focusing can be used to ensure passage of the cells in the center of the channel only. In this way, the influence of the cell trajectory with respect to the electrodes is eliminated, and cell size together

with the dielectric properties becomes the main factor determining signal amplitude rather than the exact cell trajectory. The differential detection principle based on two closely placed detection volumes, one serving as a reference, has been previously established in our group for microchip flow cytometry.[14,23] This approach considerably reduces noise and drift, and gives an accurate particle speed measurement.

Fig. 3b shows that different changes in the cell's electrical characteristics lead to different changes in the impedance spectrum. An increase in volume fraction essentially increases the signal proportionally, and hence leads to a signal increase across the entire spectrum (panel 1). Specific changes to membrane resistance, capacitance or cytosol resistance are seen in progressively higher frequency regions, as shown by the panels 2 to 4 in ascending order, although it must be said that at all but very low medium conductivities, the sensitivity to membrane resistance changes is very small.

With this microfabricated flow cytometer the detection of *Babesia bovis* infected red blood cells using impedance spectroscopy was achieved. The cellular modifications caused by the intracellular parasite result in a shift in impedance, as illustrated in Fig. 4. This can be seen directly from the scatterplots obtained by plotting imaginary *vs.* real signal components both measured at a frequency of 8.7 MHz (Fig. 4b for an infected sample, Fig. 4d for a non-infected control sample). The phase angle distribution is widened due to the appearance of additional populations upon infection (Fig. 4a *vs.* Fig. 4c). These additional populations correspond to dead red blood cells, referred to also as ghosts, for
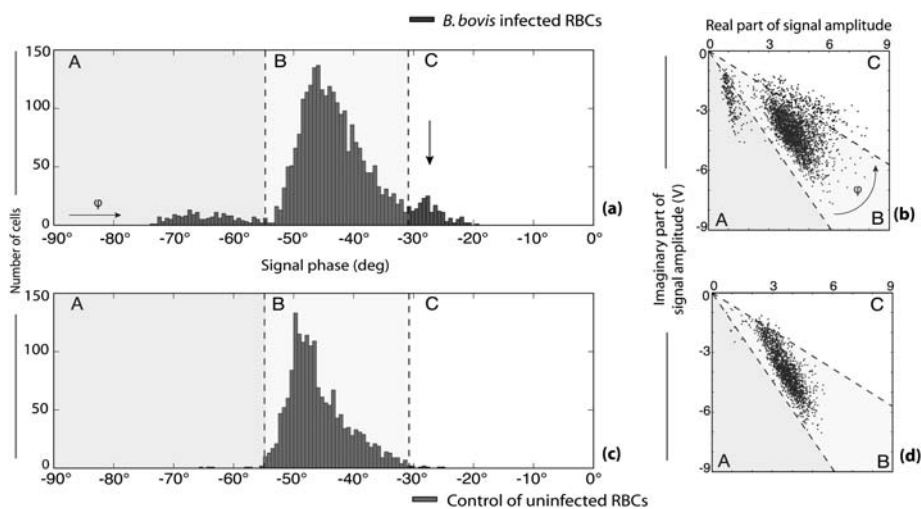
Fig. 4 Analysis of histograms yields detection of parasitized cell subpopulation. Histogram of cell counts of signal phases (a) and scattergram (b) displayed for *B.bovis* infected cells. The same graphs for a negative control of healthy bovine erythrocytes (c, d) are displayed beneath. Regions A–C mark the locations of identified subpopulations of ghost RBCs, uninfected RBCs and parasitized RBCs, respectively. The peak for the parasitised RBC subpopulation which is indicated by the arrow in the histogram (a) appears between $-30°$ and $0°$ while no peak in that region appears in the histogram of the negative control (c). The population peak of the uninfected RBCs in both histograms is located at a signal phase between $-55°$ and $-30°$. At phases lower than about $-55°$, a third peak due to ghost cells can be identified in histogram (a). The angle direction is indicated in (a) and (b).

the more negative phase angles, and to infected cells for a majority of the most positive phase angles, as confirmed by comparison with heat killed red blood cells and fluorescent labelling of infected cells. These changes at high frequency indicate a variation of the dielectric properties of the cytoplasm, and potentially the cell membrane capacitance due to the intra-cellular parasite (*cf.* Fig. 3b, panels 3 and 4), and cell death due to the infection for other cells. No obvious changes in the imped-ance measurements at lower frequency range (10 kHz to 1 MHz) were observed, indicating little change in cell size and shape. *B. bovis* infected samples contained parasitized cells as well as uninfected cells. Interestingly, although a majority of signals in the "pRBC" region is indeed due to infected cells, there is also a substantial phase shift for the non-infected cells in the same direction. In practice, this facilitates detection of infection, but would make actual separation of a sample into infected and non-infected cells more difficult.

The results presented show that a rapid cell-by-cell detection with microlitre amounts of reagents is possible, providing an easy, cheap and quick diagnostic test by exploiting the changes in the dielectric properties produced by the parasites. The method focused primarily in the direct dielectric detection of the para-sitized cells without the use of a label; and although detailed extraction of model parameters concerning the internal and membrane permittivities and conductivities can be done, it is not needed for the detection of the infection.

4. Dielectric cytometry in a continuous cell sorting microdevice

The continuous cell sorting microdevice is based on the opposi-tion of a combination of several dielectrophoretic forces at multiple frequencies that discriminates between cell types according to their dielectric properties, such as the membrane permittivity and the cytoplasm conductivity. The device also makes use of liquid electrodes to ensure an homogeneous field strength across the channel height. The fields are generated by an array of liquid electrodes located in both sidewalls of a main flow channel (Fig. 5a). Cells with different dielectric response perceive different force magnitudes and are therefore continuously focused to different equilibrium positions in the flow channel (Fig. 5b), thus avoiding again the need of cell labelling as a discriminating factor.

For cell sorting purposes, we use two low-frequency signals (in the range 50 kHz to 150 kHz), one from each side that focus the cells towards the channel midline, where the force potential minimum is located. For the actual separation we superimpose a high frequency signal (typically in the MHz range) from one of the electrodes array. The strategy is based on the results obtained by impedance measurements: at low frequency, all cells experi-ence a similar, repulsive force, so that they can be focused towards the channel midline. The high frequency signal probes cell membrane capacitance and cell interior, and should therefore shift the equilibrium position for cells of different dielectric response.

The equilibrium-based separation method can also be used for flow cytometry applications in order to characterize the dielectric properties of biological samples. When using signals of two different frequencies, the equilibrium position depends on the ratio of the forces at the two frequencies (Fig. 5b), which we term opacity.[66] In general terms, the sorting structure translates the differences in the dielectric response, into a difference in lateral position.

Like impedance spectroscopy, the dielectrophoretic force is sensitive to different cellular changes in different frequency windows (Fig. 5c). Since both techniques are fundamentally dependent on the Clausius–Mossotti factor, they are generally sensitive to identical changes in similar frequency windows.

We also applied the dielectrophoretic sorting method to the isolation on chip of *Babesia bovis* infected RBCs. Due to the
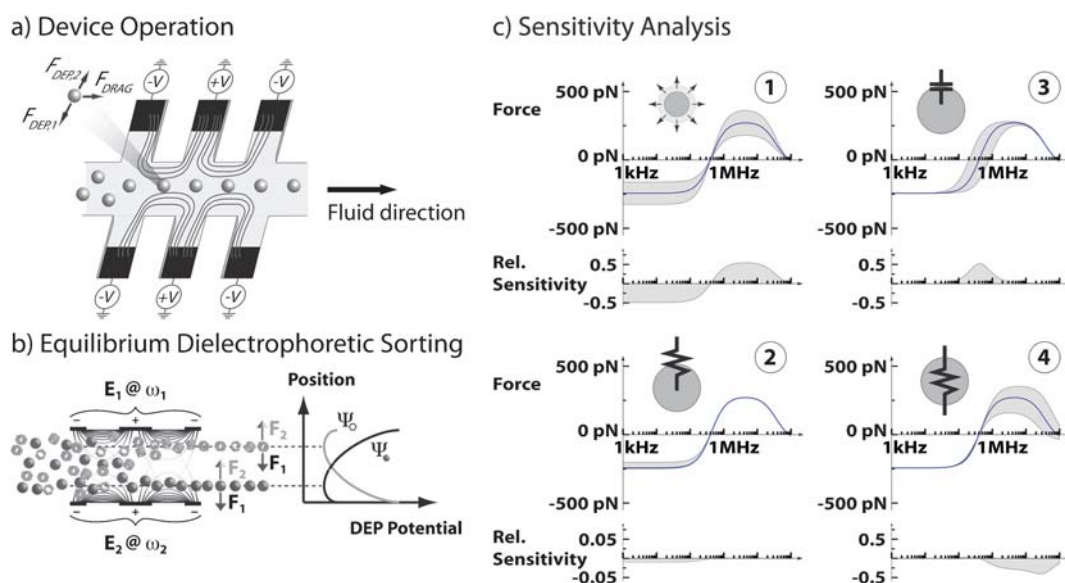
Fig. 5 (a) Schematic drawing of the cell sorting device. (b) Cell sorting principle by multiple frequency dielectrophoresis; the illustration shows a case where signals at two frequencies applied from the two liquid electrode arrays are sufficient to differentiate the cells. In many practical cases, include sorting of infected and non-infected red blood cells, we use a total of three different frequencies so that on one side, a linear combination of signals at frequencies is acting. This allows to take advantage of the sensitivity of the high frequency signals while ensuring a total nDEP force to avoid cells being drawn into the electrodes. (c) Illustration of the influence on the different model parameters on the dielectrophoretic force. The changes for each panel are identical to the changes used for Fig. 3c; for the dimensionless sensitivity, eqn (9) is used for panel 1. For panels 2–4, the change in the real part of the Clausius–Mossotti factor (*cf.* eqn (9)) is divided by the relative change of the concerned parameter, to obtain a sensitivity value that is to a first approximation independent of the actual relative parameter change. Erms = 20 V, |Erms|^2 in the channel midline as calculated from the conformal mapping, particle radius = 2.7 μm.

infection, ion loss through the cell membrane occurs and this gives a lower intracellular conductivity for the infected cells. Also the presence of the parasite itself inside the cell has an influence blocking the current flow. When sorting infected from non-infected red blood cells we observe a lower pDEP force for the infected cells, in agreement with the impedance measurements revealing a more resistive electrical behaviour. Fig. 6 shows the histogram of a separation obtained by applying a combination of signals at 90 KHz and 4MHz and a 60 KHz signal at the other side. Rather than a clean separation, an effect of enrichment of infected cells on one side of the channel and a population almost free of infected cells on the other side is observed, achieving

a final infection rate of 50% in the enriched sample. This rivals with the best available results in the literature on isolation of *B. bovis* infected cells by label-free techniques.[67]

Our separation method brings novelty and improved performances compared to the state-of-the-art of continuous-flow DEP-based cell separation for lab-on-a-chip application. The equilibrium-based sorting implies that the output positions of the particles are independent of their initial positions, upstream from the electrode array, and thus prevents resorting to a focusing step prior to separation, such as a sheath flow. Moreover, the cells quickly reach the equilibrium position and remain on the equilibrium line thanks to the laminar flow. Therefore, the cell
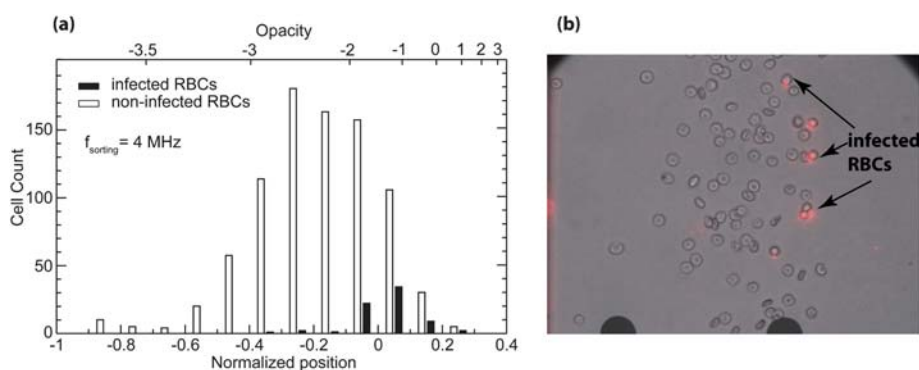
Fig. 6 Enrichment of red blood cells parasitized by *B. bovis*. The high frequency signal causes pDEP for all cells but pDEP is stronger for non-infected than for infected cells. The low frequency signals are 9.0 Vrms at 90 kHz from the left and 6.8 Vrms at 60 kHz acting from the right. In Fig. 6B, we add a high frequency signal of 4.7 Vrms at 4 MHz to the 90 kHz signal.

deviation imparted by the DEP-forces becomes independent of the flow velocity. Moreover, since the dielectrophoretic force exerted on the cells is perpendicular to the flow direction this facilitates the observation and consequently the cell position readout that is assigned to the cells' dielectric properties.

We provide an easy-to-use microchip that achieves a separation efficiency exceeding the performances of the other DEP-based methods for continuous sorting reported so far.

5. Conclusions and discussion

The experimental detection of *B. bovis* infected red blood cells and their enrichment by dielectrophoretic sorting illustrate the differences and similarities of the two techniques. Both yield an estimate of the induced dipole moment and hence the electrical changes occurring upon infection, but both have their limitations and advantages. We shall discuss some of these advantages and limitations here, a more complete list can be found in Table 1. In both cases, a simple planar fabrication technology based on liquid electrodes is used to obtain reliably operating, robust chips. Clearly, the dielectrophoretic sorting requires less expensive and complicated periphery, and automatically yields sorted, or at least enriched populations without the need for real time activation systems. It is enough to produce the required set of electrical signals in the kHz to MHz range and couple them into the chip. In impedance spectroscopy, similar input signals are required, but there is an additional stage of analogical and then digital signal amplification and treatment; in order to obtain sorting, sophisticated real-time data-treatment and actuation is needed.[68]

On the other hand, impedance spectroscopy enables rapid and convenient data acquisition; moreover it offers additional information since it is also phase sensitive. Classical dielectrophoresis as used in our equilibrium-based continuous sorter only yields information on the real part of the Clausius–Mossotti factor, whereas impedance spectroscopy yields both the real and imaginary part. The phase information acquired at a single frequency may be the most sensitive measure of a change in dielectric properties. Indeed, this is the case with the *B. bovis* infected red blood cells, which is why in Fig. 4 we report real and imaginary components at 8.7 MHz rather than a combination at multiple frequencies. In other cases, combinations of signals at different frequencies yield a more sensitive description of the cells; the important point in impedance spectroscopy is that we have the freedom to choose among phase and magnitude information of different frequency channels to obtain the most sensitive measure of the system under study.

In equilibrium-based dielectrophoretic sorting, on the other hand, we obtain the opacity as a measure of the relative response of the cell at two different frequencies. More precisely, we obtain the ratio of the real parts of the Clausius–Mossotti factor at the low and high frequency. We do not have the freedom to observe the imaginary parts at the two frequencies, the phase, or more exotic combinations of different channels. However, since phase and amplitude information are related by the Kramers–Kronig relations, it is generally possible to obtain a sensitive measurement using suitably chosen frequencies. For instance, for the enrichment of *B. bovis* infected cells, we use the low frequency signal as a normalization for cell size, while the high frequency-signal actually probes the cell interior and detects conductivity

Table 1 Dielectric cytometry: Impedance Flow cytometer *vs.* Dielectrophoretic Cell sorting[a]

Properties	Impedance flow cytometer	Dielectrophoretic Sorting
Method	Impedance spectroscopy	Dielectrophoresis
	Measure at multiple frequencies (100KHz to 15MHz)	Multiple frequencies
		Equilibrium positions
	Measures ΔZ	Measures Δx
	Real and imaginary part of impedance	Real part of f_{CM}
Electrical		
Electric-field form	+++ (vertical equipotential surface, well defined)	+++ (vertical equipotential surface, well defined)
Electrode surface	++ Large area	++ Large area
Electrode material	Platinum	Platinum
Sensitivity	+++	+++
Efficiency	+++	+++
Reproducibility	+	+++
Optical		
in situ visualization	+	+++
Real time monitoring	++	+++
Others		
Microfabrication	+++ (simple technology)	+++ (simple technology)
Sample volume	Small, dilution of samples	Small
Sample pre-treatment	Not needed	Not needed
Cell handling	+	+++
Flow control and particle speed	Needs to be precise	Independent to a large extent
Medium conductivity	+++ (physiological media)	+ (low K)
Throughput	++	+++ (high), parallelization
Integration	+++	+++
Disposability	+++	+++
Cost	++	++

[a] +++: high or excellent; ++: medium or good; +: low or poor.

changes due to the presence of the parasite. The resistive and capacitive changes responsible for the phase shift in impedance spectroscopy then lead to an altered force ratio between high and low frequency. In addition, if needed, it would be possible to use travelling-wave dielectrophoresis[57] or electrorotation[69] to estimate the imaginary component of the cell polarization.

Both the impedance spectroscopy microdevices and the equilibrium dielectrophoretic sorter are application-ready. We have successfully used the impedance spectroscopy approach to characterize red blood cells, ghosts, and different types of white blood cells in addition to the detection of *B. bovis* infection, whereas the equilibrium dielectrophoretic sorter has made its proof not only in enrichment of *B. bovis* infected red blood cells, but also in the separation of viable and non-viable yeast cells as well as the synchronization of a yeast cell culture.[70,71] In essence, the two techniques represent flow-through whole-cell patch-clamping: we obtain an electrical characterization of the cells during the short period they spend in the measurement volume. The difference is that impedance spectroscopy allows complete and rapid data acquisition, while the equilibrium-based sorter yields sorted populations.

Finally, for future developments, the equilibrium dielectrophoretic sorting principle in particular has interesting perspectives in high-throughput applications: since no signal processing is required for the sorting process *per se*, potentially large scale parallelization should be possible.

6. Outlook

The on chip impedance and dielectrophoretic force spectroscopy technique presented here is a ready-to-use tool in point-of-care diagnosis applications for cell counting and separation in fields as hematology, oncology and toxicology. Moreover, the technique is label-free and non-invasive, avoiding any cell modification and allowing further studies on the sample, which is of great interest in areas such as immunology and in stem cell differentiation studies. As the dielectric properties of cells are sensitive to external stimuli such as drug exposure and bacterial or viral infections, the technology is also very suitable for cell cycle analysis, apoptosis and toxicity/viability studies. Impedance spectroscopy flow cytometry can be a valuable alternative to conventional fluorescence-activated cell sorter (FACS) as has been proved for whole-cell analyses,[25] and also for discrimination of various cell line types, such as undifferentiated mouse fibroblasts 3T3-L1 and adipocytes on the one hand, or human monocytes and *in vitro* differentiated dendritic cells and macrophages on the other hand.[72,73]

Moreover, for those applications in which no specific cell markers are known or where fluorescent labels fail, impedance spectroscopy could be an option. Since it is a label free technique, costs of assays as well as the time needed for sample preparation get significantly reduced and therefore this technique can assist in different cell analyses performed today by the FACS instrument.

References

1 D. W. Bianchi and J. Hanson, *J. Maternal-Fetal. Neonatal Med.*, 2006, **19**, 199–207.
2 M. Kersaudy-Kerhoas, R. Dhariwal and M. P. Y. Desmulliez, *IET Nanobiotechnol.*, 2008, **2**, 1–13.
3 W. R. Rodriguez, N. Christodoulides, P. N. Floriano, S. Graham, S. Mohanty, M. Dixon, M. Hsiang, T. Peter, S. Zavahir, I. Thior, D. Romanovicz, B. Bernard, A. P. Goodey, B. D. Walker and J. T. McDevitt, *PLoS Med.*, 2005, **2**, 663–672.
4 L. J. Yang, P. P. Banada, M. R. Chatni, K. S. Lim, A. K. Bhunia, M. Ladisch and R. Bashir, *Lab Chip*, 2006, **6**, 896–905.
5 N. Bao, J. Wang and C. Lu, *Anal. Bioanal. Chem.*, 2008, **391**, 933–942.
6 N. Fertig, R. H. Blick and J. C. Behrends, *Biophys. J.*, 2002, **82**, 3056–3062.
7 N. Fertig, C. Meyer, R. H. Blick and J. C. Behrends, Coupling of Biological and Electronic Systems, 2002, pp. 29–40.
8 C. Schmidt, M. Mayer and H. Vogel, *Angew. Chem.-Int. Ed.*, 2000, **39**, 3137–3140.
9 J. El-Ali, P. K. Sorger and K. F. Jensen, *Nature*, 2006, **442**, 403–411.
10 G. Cellot, E. Cilia, S. Cipollone, V. Rancic, A. Sucapane, S. Giordani, L. Gambazzi, H. Markram, M. Grandolfo, D. Scaini, F. Gelain, L. Casalis, M. Prato, M. Giugliano and L. Ballerini, *Nat. Nanotechnol.*, 2009, **4**, 126–133.
11 B. J. Dworak and B. C. Wheeler, *Lab Chip*, 2009, **9**, 404–410.
12 A. Hai, J. Shhappir and M. E. Spira, *Nat. Methods*, 2010, **7**, 200–210.
13 W. H. Coulter, *Proc. Natl. Electron. Conf.*, 1956, 12.
14 S. Gawad, L. Schild and P. Renaud, *Lab Chip*, 2001, **1**, 76–82.
15 R. A. Hoffman and W. B. Britt, *J. Histochem. Cytochem.*, 1979, **27**, 234–240.
16 R. A. Hoffman, T. S. Johnson and W. B. Britt, *Cytometry*, 1981, **1**, 377–384.
17 D. Holmes, D. Pettigrew, C. H. Reccius, J. D. Gwyer, C. van Berkel, J. Holloway, D. E. Davies and H. Morgan, *Lab Chip*, 2009, **9**, 2881–2889.
18 H. Morgan, T. Sun, D. Holmes, S. Gawad and N. G. Green, *J. Phys. D: Appl. Phys.*, 2007, **40**, 61–70.
19 K. R. Foster and H. P. Schwan, *Crit. Rev. Biomed. Eng.*, 1989, **17**, 25–104.
20 H. Fricke, *J. Gen. Physiol.*, 1925, **9**, 137–152.
21 R. Pethig and D. B. Kell, *Phys. Med. Biol.*, 1987, **32**, 933–970.
22 H. P. Schwan, *Adv. Biol. Med. Phys.*, 1957, **5**, 147–209.
23 S. Gawad, K. Cheung, U. Seger, A. Bertsch and P. Renaud, *Lab Chip*, 2004, **4**, 241–251.
24 H. E. Ayliffe, A. B. Frazier and R. D. Rabbitt, *J. Microelectromech. Syst.*, 1999, **8**, 50–57.
25 K. Cheung, S. Gawad and P. Renaud, *Cytometry, Part A*, 2005, **65A**, 124–132.
26 Y. H. Cho, T. Yamamoto, Y. Sakai, T. Fujii and B. Kim, *J. Microelectromech. Syst.*, 2006, **15**, 287–295.
27 D. Holmes, H. Morgan and N. G. Green, *Biosens. Bioelectron.*, 2006, **21**, 1621–1630.
28 D. Holmes, M. E. Sandison, N. G. Green and H. Morgan, Micro Total Analysis Systems 2004, 2005, **vol. 1**, pp. 6–8.
29 H. Morgan, D. Holmes and N. G. Green, *Curr. Appl. Phys.*, 2006, **6**, 367–370.
30 M. Nelson, *Pathology*, 1999, **31**.
31 Z. Palkova, L. Vachova, M. Valer and T. Preckel, *Cytometry, Part A*, 2004, **59A**, 246–253.
32 L. L. Sohn, O. A. Saleh, G. R. Facer, A. J. Beavis, R. S. Allan and D. A. Notterman, *Proc. Natl. Acad. Sci. U. S. A.*, 2000, **97**, 10687–10690.
33 J. Suehiro, R. Yatsunami, R. Hamada and M. Hara, *J. Phys. D: Appl. Phys.*, 1999, **32**, 2814–2820.
34 H. Tang and Y. F. Gao, *IEEE Sens. J.*, 2005, **5**, 1346–1352.
35 B. Yao, G. A. Luo, X. Feng, W. Wang, L. X. Chen and Y. M. Wang, *Lab Chip*, 2004, **4**, 603–607.
36 P. R. C. Gascoyne and J. Vykoukal, *Electrophoresis*, 2002, **23**, 1973–1983.
37 M. P. Hughes, *Electrophoresis*, 2002, **23**, 2569–2582.
38 T. Braschler, N. Demierre, E. Nascimento, T. Silva, A. G. Oliva and P. Renaud, *Lab Chip*, 2008, **8**, 280–286.
39 N. Demierre, T. Braschler, P. Linderholm, U. Seger, H. van Lintel and P. Renaud, *Lab Chip*, 2007, **7**, 355–365.
40 N. Demierre, T. Braschler, R. Muller and P. Renaud, *Sens. Actuators, B*, 2008, **132**, 388–396.
41 R. Pethig, *Crit. Rev. Biotechnol.*, 1996, **16**, 331–348.
42 M. Borgatti, L. Altomare, M. Baruffa, E. Fabbri, G. Breveglieri, G. Feriotto, N. Manaresi, G. Medoro, A. Romani, M. Tartagni, R. Gambari and R. Guerrieri, *Int. J. Mol. Med.*, 2005, **15**, 913–920.

43 P. R. C. Gascoyne, X. B. Wang, Y. Huang and F. F. Becker, *IEEE Trans. Ind. Appl.*, 1997, **33**, 670–678.

44 G. H. Markx, M. S. Talary and R. Pethig, *J. Biotechnol.*, 1994, **32**, 29–37.

45 L. M. Yu, C. Iliescu, G. L. Xu and F. E. H. Tay, *J. Microelectromech. Syst.*, 2007, **16**, 1120–1129.

46 I. Doh and Y. H. Cho, *Sens. Actuators, A*, 2005, **121**, 59–65.

47 Y. Huang, X. B. Wang, F. F. Becker and P. R. C. Gascoyne, *Biophys. J.*, 1997, **73**, 1118–1129.

48 Y. L. Li, C. Dalton, H. J. Crabtree, G. Nilsson and K. V. I. S. Kaler, *Lab Chip*, 2007, **7**, 239–248.

49 G. H. Markx, R. Pethig and J. Rousselet, *J. Phys. D: Appl. Phys.*, 1997, **30**, 2470–2477.

50 T. Muller, T. Schnelle, G. Gradl, S. G. Shirley and G. Fuhr, *J. Liq. Chromatogr. Relat. Technol.*, 2000, **23**, 47–59.

51 L. M. Barrett, A. J. Skulan, A. K. Singh, E. B. Cummings and G. J. Fiechtner, *Anal. Chem.*, 2005, **77**, 6798–6804.

52 C. F. Chou and F. Zenhausern, *IEEE Eng. Med. Biol. Mag.*, 2003, **22**, 62–67.

53 K. H. Kang, Y. J. Kang, X. C. Xuan and D. Q. Li, *Electrophoresis*, 2006, **27**, 694–702.

54 B. H. Lapizco-Encinas, B. A. Simmons, E. B. Cummings and Y. Fintschenko, *Anal. Chem.*, 2004, **76**, 1571–1579.

55 S. Masuda, M. Washizu and T. Nanba, *IEEE Trans. Ind. Appl.*, 1989, **25**, 732–737.

56 G. De Gasperis, J. Yang, F. F. Becker, P. R. C. Gascoyne and X. B. Wang, *Biomed. Microdevices*, 1999, **2**, 41–49.

57 H. Morgan, N. G. Green, M. P. Hughes, W. Monaghan and T. C. Tan, *J. Micromech. Microeng.*, 1997, **7**, 65–70.

58 M. S. Talary, J. P. H. Burt, J. A. Tame and R. Pethig, *J. Phys. D: Appl. Phys.*, 1996, **29**, 2198–2203.

59 K. Asami, *Prog. Polym. Sci.*, 2002, **27**, 1617–1659.

60 K. Asami, *J. Non-Cryst. Solids*, 2002, **305**, 268–277.

61 H. P. Schwan and C. F. KAY, *Ann. N. Y. Acad. Sci.*, 1957, **65**, 1007–1013.

62 H. P. Schwan and C. F. KAY, *Circulation Research*, 1957, **5**, 439–443.

63 A. Irimajiri, T. Hanai and A. Inouye, *J. Theor. Biol.*, 1979, **78**, 251–269.

64 H. Morgan and N. G. Green, *AC Electrokinetics: Colloids and Nanoparticles*, Research Studies Press, Baldoch, Hertfordshire, UK, 2002.

65 J. Gimsa and D. Wachner, *Biophys. J.*, 1998, **75**, 1107–1116.

66 A. Valero, T. Braschler, N. Demierre and P. Renaud, *Biomicrofluidics*, 2010, **4**, 022807–022809.

67 S. D. Rodriguez, G. M. Buening, C. A. Vega and C. A. Carson, *Exp. Parasitol.*, 1986, **61**, 236–243.

68 S. Gawad, PhD thesis, EPFL, 2004.

69 M. Kriegmaier, M. Zimmermann, K. Wolf, U. Zimmermann and V. L. Sukhorukov, *Biochim. Biophys. Acta, Gen. Subj.*, 2001, **1568**, 135–146.

70 T. Braschler, PhD thesis, EPFL, 2009.

71 N. Demierre, PhD thesis, EPFL, 2008.

72 G. Schade-Kampmann, M. Hebeisen, A. Huwiler, T. Hessler and M. Di Berardino, *Cytometry Part A*, 2007, **71A**, 765–766.

73 G. Schade-Kampmann, A. Huwiler, M. Hebeisen, T. Hessler and M. Di Berardino, *Cell Proliferation*, 2008, **41**, 830–840.

74 P. Gascoyne, J. Satayavivad and M. Ruchirawat, *Acta Trop.*, 2004, **89**, 357–369.